

# Investigations on ZnO Thin Films Modified with Urea: An Approach as Ammonia Sensor

Venkata Satya Chidambara Swamy Vaddadi, Saidi Reddy Parne,\* Nagaraju Pothukanuri,\* Srinivasa Rao Sriram, and Vijayakumar Yelsani



Cite This: *ACS Omega* 2023, 8, 17719–17730



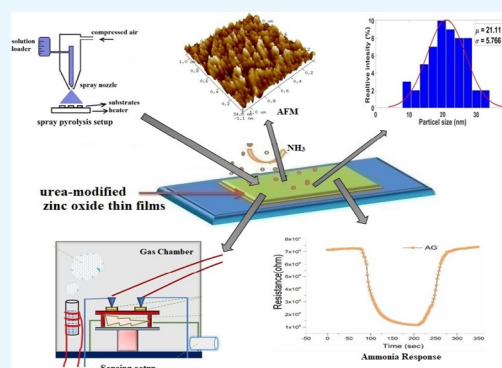
Read Online

ACCESS |

Metrics & More

Article Recommendations

**ABSTRACT:** Pure and urea-modified zinc oxide thin films are prepared using the spray pyrolysis technique on microscopic glass substrates. We have added different urea concentrations as a modifier to the zinc acetate precursor for obtaining urea-modified ZnO thin films and investigated the effect of the urea concentration on the structural, morphological, optical, and gas-sensing properties. The gas-sensing characterization of pure and urea-modified ZnO thin films is tested in the static liquid distribution technique with 25 ppm of ammonia gas at an operating temperature of 27 °C. The prepared film with a concentration of 2 wt % of urea has shown the best sensing properties toward ammonia vapors due to more active sites for the reaction between chemisorbed oxygen and the target vapors.



## 1. INTRODUCTION

Rapid economic development and industrialization have caused global environmental issues in the recent past. Ammonia is a reducing and colorless gas produced from refrigerators, industrial emissions, and food processing companies, leading to ecological imbalances.<sup>1</sup> Long-term exposure to ammonia gas at concentrations of more than 5000 ppm will damage the human health system. It can cause serious health issues for a long time in the body and can even drag the person to death.<sup>2</sup> According to the safety and health measurements, the permissible limitation of ammonia is 300 ppm.<sup>3</sup> Higher concentration of ammonia can damage the growth, the immune system, and the reproduction cycle of animals and humans. Hence, the enhanced demand for ammonia gas sensors at room temperature with low concentrations is an immediate requirement in food processing technology, chemical industry, fertilizers, environmental, automotive, and medical applications. Over the last few decades, research has been carried out to detect ammonia gas using optical sensors,<sup>4,5</sup> electrochemical sensors,<sup>6</sup> and surface acoustic wave sensors<sup>7</sup> which are costly and time-consuming processes. The chemiresistive technique is a cost-effective technique with good stability and repeatability. In chemiresistive gas sensing, variation in resistance can be measured in the presence of the target analyte, and the material of the sensing layer would be significant.<sup>8</sup>

Mesoporous metal oxide-based materials such as  $\text{WO}_3$ , ZnO,  $\text{SnO}_2$ , and  $\text{TiO}_2$  have become significant materials in sensor devices due to their lightweight and high active surface area to interact with gas molecules.<sup>9,10</sup> Zinc oxide is a distinctive

material that shows piezoelectric, semiconducting, microbial, optical, and pyroelectric properties. Zinc oxide (ZnO) is an n-type semiconductor, and it has a Wurtzite structure with an optical band gap value of 3.37 eV. It also possesses a high excitation binding energy of 60 meV at room temperature. These unique properties make ZnO suitable for sensor devices.<sup>11,12</sup> Various synthesis techniques are involved in preparing ZnO nanostructures, such as chemical vapor coating,<sup>13</sup> sol-gel method,<sup>14</sup> electrochemical deposition,<sup>15</sup> sputtering,<sup>16</sup> hydrothermal,<sup>17</sup> and spray pyrolysis technique.<sup>18</sup> The surface morphology, crystal type, crystal size, particle shape, particle size distribution, degree of agglomeration, and porosity are explored as properties of nanostructures that make them appropriate for gas-sensing applications. Wang et al.<sup>19</sup> reported the preparation of ZnO nanoparticles using a solvothermal technique at 180 °C for 24 h using zinc acetate dihydrate  $[\text{Zn}(\text{CH}_3\text{CO}_2)_2 \cdot 2\text{H}_2\text{O}]$  and urea. They have reported that the particle size ranges from 50 to 200 nm. Hu et al.<sup>20</sup> synthesized nanocrystalline ZnO particles using an aqueous solution of zinc acetate dihydrate and urea using the hydrothermal method at 120 °C for 2–4 h, and further, the obtained precursor was calcinated in the temperature range of 350–650 °C for 30–120

Received: January 14, 2023

Accepted: May 4, 2023

Published: May 12, 2023



min. Due to the calcination process, different grain shapes and crystallite sizes of ZnO nanoparticles were obtained. Marinho et al.<sup>21</sup> prepared ZnO nanostructures with normal water bath heating and a microwave hydrothermal technique in an aqueous solution with zinc acetate and urea as essential components. They reported that well crystalline ZnO nanostructures with various morphologies were obtained using the urea precursor. The formation of ZnO is due to the nucleation mechanism and the prominent growth direction of the crystal. Liu et al.<sup>22</sup> prepared ZnO nanoparticles using urea and zinc nitrate precursors using the homogeneous precipitation method. This article shows a significant impact of urea on the morphology and porosity of ZnO nanoparticles. Most research articles presented in the literature focused on the preparation of materials using urea as a modifier/dopant for structural, morphological, chemical, and optical properties.

As far as we know, this is the maiden effort to study the gas-sensing properties of zinc oxide thin films modified using urea. In this investigation, we have deposited pure and modified zinc oxide thin films with various urea concentrations using the spray pyrolysis deposition technique. We have noticed from the latest literature review that urea acts as an excellent modifier which eliminates agglomeration during the deposition process and controls the structural, morphological, and optical properties, in turn improving the gas-sensing properties.<sup>21</sup> However, the currently accessible metal oxide-based sensors to detect ammonia vapors require more maintenance and work at high operating temperatures. Hence, there is an urgent need to make an ammonia sensor working at room temperature with low cost and high chemical stability.

## 2. EXPERIMENTAL TECHNIQUES

**2.1. Materials.** Zinc acetate dihydrate  $[\text{Zn}(\text{CH}_3\text{CO}_2)_2 \cdot 2\text{H}_2\text{O}]$  and urea were used as starting ingredients and were obtained from Sigma Aldrich in India.

**Table 1. Deposition Conditions**

s.no	deposition parameters	details
1	precursors	zinc acetate and urea
2	solvents	deionized water and methanol
3	substrates	microslides, Blue star-India
4	deposition time	15 min
5	NSD	25 cm
6	substrate temperature	425 °C
7	concentration of precursor	0.25 M
8	flow rate	2 mL/min

**2.2. Preparation of ZnO Thin Film Samples.** Zinc acetate dihydrate  $\text{Zn}(\text{CH}_3\text{CO}_2)_2 \cdot 2\text{H}_2\text{O}$  was dissolved in deionized water and methanol in the same ratio using a magnetic stirrer continuously for 90 min at room temperature to obtain a transparent solution. Before deposition, the glass substrates were cleaned thoroughly in three steps. First, they were washed with a particle-free solution for 10 min to remove dust particles; second, they were cleaned with deionized water to remove ionic particles on the glass substrate so that they do not react with the coating materials; third, they were cleaned with an ultrasonicator for 20 min and later dried in a hot air oven. The above-obtained solution was sprayed on pre-cleaned glass substrates to prepare pure ZnO films using computer interfaced spray pyrolysis (Holmarc, India, model number HO-TH-04BT) method, with the optimized deposition conditions depicted in Table 1.

Furthermore, to study the effect of urea concentration, 2, 4, and 6 wt % of nontoxic urea ( $\text{CH}_4\text{N}_2\text{O}$ ) were added to the zinc acetate precursor solution separately and mixed for about 90 min. After obtaining a clear solution, urea-modified ZnO thin films were coated on a glass substrate by the spray pyrolysis deposition method, and the obtained films were labeled as AE (pure ZnO), AF (2 wt % of urea), AG (4 wt % of urea), and AH (6 wt % of urea) for further characterization.

**2.3. Fabrication of Sensing Element.** To investigate the gas-sensing properties of the prepared zinc oxide films, silver paste and copper wires were used to manufacture ohmic connections on the two ends of the thin film surface with a 1 cm separation. To ensure proper contact with the electrodes, these sensor parts were heated for 2 h at 150 °C. The gas-sensing characteristics of these films were investigated at room temperature using a concentration of 25 ppm of ammonia in the static mode. A schematic gas-sensing system is shown in Figure 1.

**2.4. Characterization Techniques.** The weight difference technique was used to calculate the thickness of the films. The samples' morphological, structural, and optical properties were investigated using different characterization techniques such as X-ray diffraction analysis (XRD), scanning electron microscopy (SEM), high-resolution transmission electron microscopy (HRTEM), atomic force microscopy (AFM), Raman spectroscopy, and UV-vis spectroscopy. A Bruker (D8 Advance, Germany) X-ray diffractometer was used to perform XRD with  $\text{CuK}\alpha$  (1.54 Å) radiation in the grazing incidence mode and the wide-angle ( $2\theta$ ) range of 20 to 80°. The film's root-mean-square (RMS) roughness was characterized by AFM (Bruker) in the contact mode with 0.5 Hz frequency. The morphology of the films was studied by a Hitachi (TM 4000) scanning electron microscope using an accelerating voltage of 15 kV and a working distance of 6 mm, and compositional analysis of the sample was performed with energy-dispersive X-ray spectroscopy. The thin films' nanostructured nature was studied HRTEM (JEOL). Raman spectra were obtained using a LAB RAM HR Raman spectrometer at room temperature with excitation of 532 nm emission from an Nd-YAG laser of power 100 mW at 50× magnification with a resolution of 8  $\text{cm}^{-1}$ . During the analysis, baseline reduction and minimal smoothing were also used. Optical studies were analyzed by a UV-vis spectrophotometer (Jasco V770). Using an indigenously made setup, gas-sensing characterization was carried out with a Keithley's (6517B) electrometer.

## 3. RESULTS AND DISCUSSION

**3.1. Thickness Measurement.** The thickness of the prepared thin films was determined using the weight difference procedure with the following formula.<sup>23</sup> The thickness of the films is found to reduce due to the addition of urea. The decrease in the thickness of the thin films prepared with urea concentrations may be due to the excessive amount of  $\text{NH}_4^+$  generated. The excess  $\text{NH}_4^+$  generated with high concentrations of urea can negatively affect the growth of ZnO-based nanostructures.<sup>24</sup> The calculated thicknesses are listed in Table 4.

$$\text{Thickness of the film } (t) = \frac{\Delta m}{\alpha a}$$

where  $\Delta m$  is the variation in the weight of the sample before and after the deposition,  $\alpha$  is the standard density of the zinc oxide material, and 'a' is the area of the substrate.

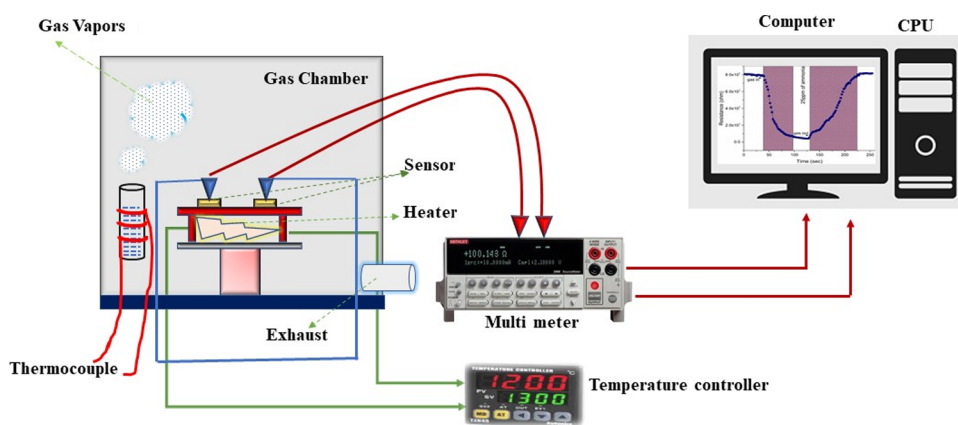


Figure 1. Schematic of the gas-sensing system.

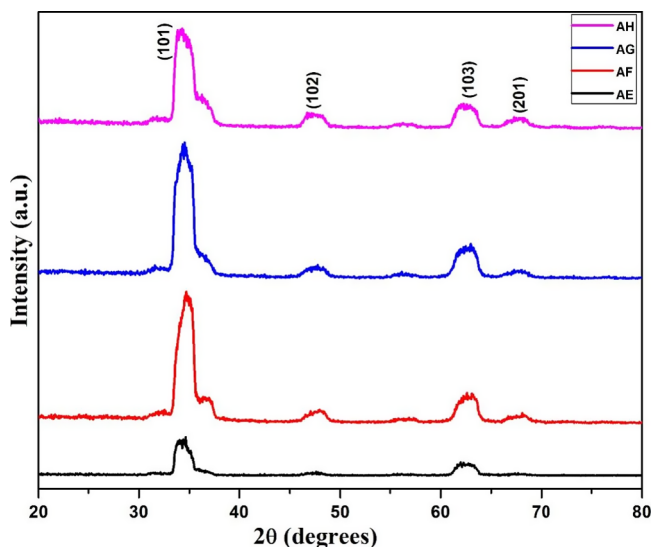


Figure 2. XRD spectra of pure and urea-modified ZnO thin films.

**3.2. XRD Analysis.** The thin films' phase identification, structural characteristics, and crystallite size were all determined using XRD. The XRD pattern of pure and modified ZnO thin films using different urea concentrations is shown in Figure 2. The XRD pattern shows polycrystalline ZnO thin films with the characteristic peaks  $2\theta = 34.25, 47.28, 62.60,$  and  $67.68^\circ$  ascribed to the distinct planes of (101), (102), (103), and (201) of zinc oxide, which is correlated with the JCPDS card number 075-1533 and confirms the Wurtzite phase of hexagonal ZnO.<sup>25</sup> There are no other diffraction peaks detected in the samples. Due to the high substrate temperature, adding urea to the zinc source did not affect the development of ZnO nanostructures.<sup>26,27</sup> The peak broadening indicates that the nanocrystalline phase exists in the prepared samples.

The interplanar spacing is determined with the following relation.<sup>28</sup>

$$\frac{1}{d^2} = \frac{4}{3} \left( \frac{h^2 + hk + k^2}{a^2} \right) + \frac{l^2}{c^2}$$

$h, k,$  and  $l$  are miller indices;  $a$  and  $c$  are lattice constants.

The lattice constants  $a$  and  $c$  are determined using the following equation<sup>29,30</sup> along the (101) direction, and the calculated values are listed in Table 2.

$$a = \frac{\lambda}{\sqrt{3} \sin\theta}$$

$$c = \frac{\lambda}{\sin\theta}$$

The remaining structural parameters, the unit cell volume ( $V$ ) and the bond length ( $L$ ), are evaluated with the following relation, and the derived values are tabulated in Table 2.

$$L = \sqrt{\left( \frac{a^2}{3} + \left( \frac{1}{2} - u \right)^2 c^2 \right)}$$

where ' $u$ ' is called a potential parameter in the Wurtzite structure and is given by

$$u = \frac{a^2}{3c^2} + 0.25$$

The ZnO structure comprises two interpenetrating hexagonal closely packed (hcp) sublattices. In these lattices, one atom is displaced with another one along the  $c$ -axis by 0.375 [equals potential parameter ( $u$ ) in an ideal Wurtzite structure], and this is expressed as the length of the bond parallel to the  $z$ -axis. It is noted clearly that the above relation between the potential parameter ' $u$ ' and the  $c/a$  ratio is inversely proportional. If the  $c/a$  ratio reduces, the potential parameter will increase. The four

Table 2. Structural Parameters of the ZnO and Urea-Modified Zinc Oxide Films

sample	crystallite size ( $D$ ) (nm)		dislocation density $\times 10^{14}$ (lines/m <sup>2</sup> )	lattice constants		strain $\times 10^{-4}$
	XRD	TEM		$a$ (Å)	$c$ (Å)	
AE	36.41	33.89	7.54	3.01	5.22	9.99
AF	22.87	21.11	19.11	3.00	5.20	15.82
AG	25.31	25.83	15.61	2.99	5.18	14.29
AH	26.74	26.51	13.98	2.99	5.19	13.53

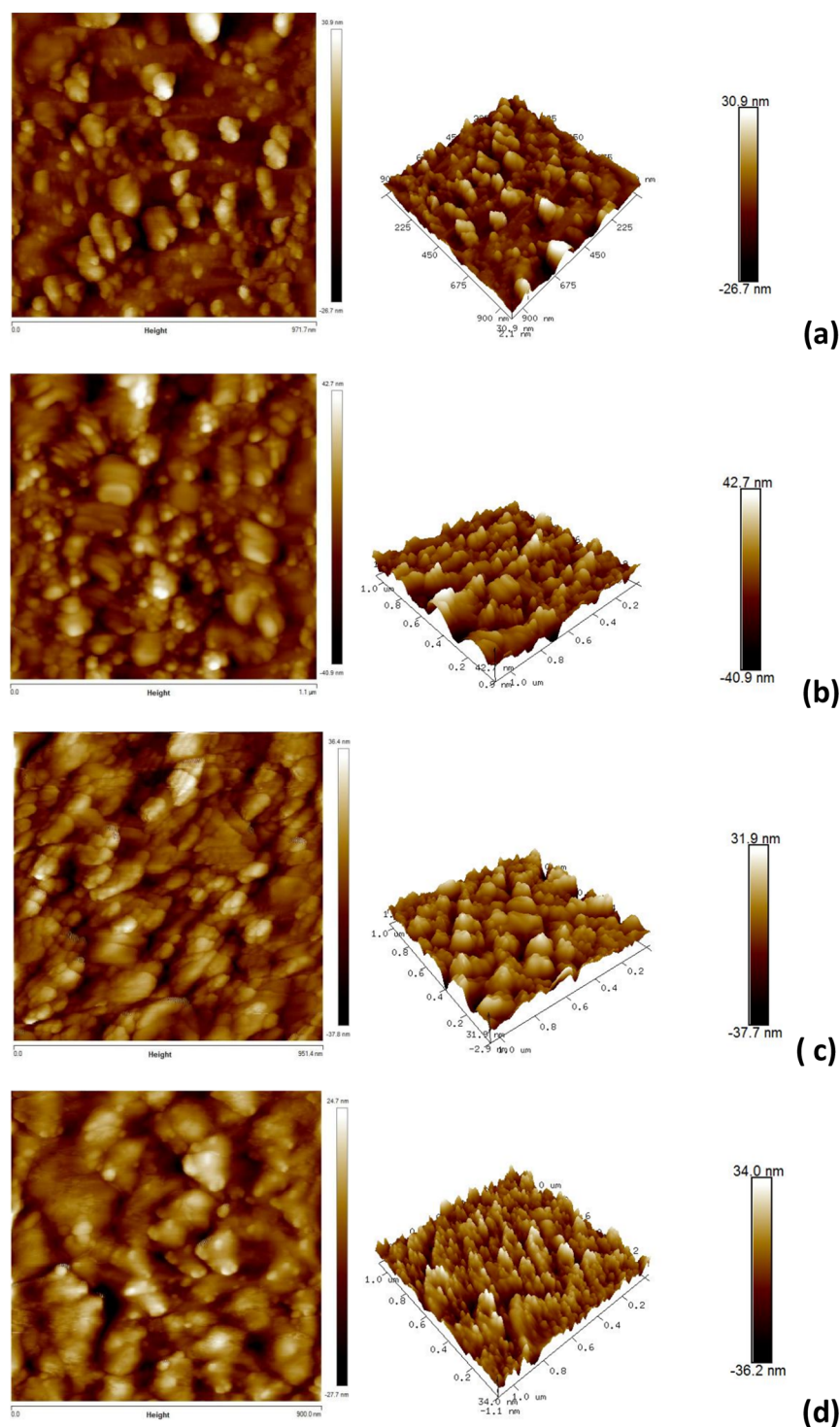


**Figure 3.** 2D and 3D AFM images of pure and urea-modified ZnO thin films. (a) Pure ZnO, (b) 2 wt % of urea, (c) 4 wt % of urea, and (d) 6 wt % of urea.

**Table 3.** Surface Features of Pure and Urea-Modified ZnO Thin Films Obtained from AFM Studies

s. no.	sample name	average roughness ( $R_a$ )	RMS roughness ( $R_q$ )	skewness	grain height (nm)
1	AE	7.56	9.78	-0.093	34.0
2	AF	3.14	4.18	0.092	17.1
3	AG	5.06	6.44	-0.133	23.0
4	AH	7.25	8.39	-0.380	31.9

tetrahedral lengths remain the same in the ZnO lattice through a distortion due to an extensive range of polar interactions.<sup>31</sup>

$$\text{Volume of the unit cell } (v) = 0.866a^2c$$

It is perceived that with the enhancing urea concentration in the zinc oxide matrix, the peaks were moved with the decreased intensity of (101) peak, and the peaks got broadened. Broadening of the peaks will increase full width at half-maximum (FWHM), which may cause the growth of the crystal grains.<sup>32</sup> It

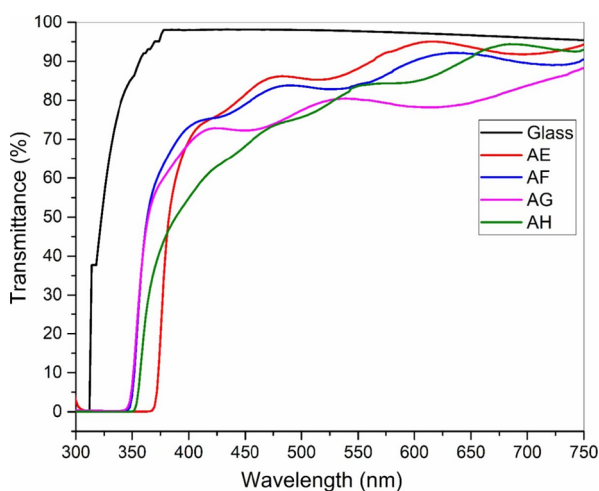


**Figure 4.** Transmittance spectra of pure and urea-modified ZnO thin films.

is also observed that (101) plane is the preferred orientation in all samples. The average crystallite size can be derived using the Scherrer formula.<sup>33</sup>

$$\text{Crystallite size } (D) = \frac{0.94\lambda}{\beta\cos\theta}$$

The calculated average crystallite sizes of pure and urea-modified ZnO thin films are charted in Table 2. Here, ' $\lambda$ ' is the wavelength of monochromatic X-rays (1.5406 Å), ' $\beta$ ' is the FWHM, and ' $\theta$ ' is the diffraction angle. Interestingly, the crystallite size decreased by adding the 2 wt % urea concentration in the ZnO source.<sup>34</sup> According to Khoshhesab et al.,<sup>35</sup> the addition of urea reduces the size of the crystal, and its polarity allows it to adsorb on the nuclei of zinc oxide crystals, preventing them from agglomerating into larger particles. Thus, the growth of the crystallites is restricted, and the enhancement in the crystallite size further is due to the predominance of particle growth during the deposition process.

Lattice strain can be calculated from the XRD analysis. It can be defined as the lattice constant distribution, such as lattice imperfections that occur from the crystal defects.<sup>36</sup> XRD data depict a shift in the peak position and variation in FWHM in all the samples deposited with different urea concentrations as correlated with the pure zinc oxide sample. This shift represents a strain produced on the host lattice during the deposition.

**Table 4.** Optical Properties of Pure and Urea-Modified ZnO Thin Films

s. no.	sample code	thickness (nm)	optical band gap (eV)
1	AE	179	3.17
2	AF	162	3.20
3	AG	144	3.22
4	AH	136	3.24

Strain caused by crystal imperfections and distortion has been determined by the Williamson-Hall relation.<sup>37</sup> The calculated strain is tabulated in Table 2.

$$\varepsilon = \frac{\beta\cos\theta}{4}$$

The crystallographic defects or irregularities can be measured within the crystal by using the crystal dislocation density. Dislocation density measures the length of dislocation lines per unit volume of the crystal and calculated using the following formula.<sup>38</sup> The calculated dislocation density value for each sample is tabulated in Table 2.

$$\delta = \frac{1}{D^2}$$

**3.3. AFM Studies.** AFM is a good characterization technique for studying the deposited thin film's texture and morphology. This technique is a model for quantitatively computing the nanoscale features and visualizing the deposited film structure. The surface roughness of thin films significantly influences the manufacturing of photoelectric devices and sensors. Therefore, roughness is an essential tool to measure before producing the devices.<sup>39</sup> A Bruker atomic force microscope was used to explore the surface topology of the deposited thin films, and nanoscope E software was used to analyze the surface topology. Figure 3 shows the 2D and 3D AFM images of pure ZnO and ZnO thin films modified with different urea concentrations, respectively. To measure the roughness, the deposited thin films are scanned with the tapping mode in the range of  $1\ \mu\text{m} \times 1\ \mu\text{m}$ . The roughness parameters are estimated by analyzing the topography of the scanned samples. The surface profile parameters include RMS and average roughness. Both are similar to others, with the only difference being the mean-squared absolute values of the surface roughness profile.<sup>40,41</sup> The average roughness of the sample is the mean height determined over the total measured length, and it is utilized to narrate the roughness of

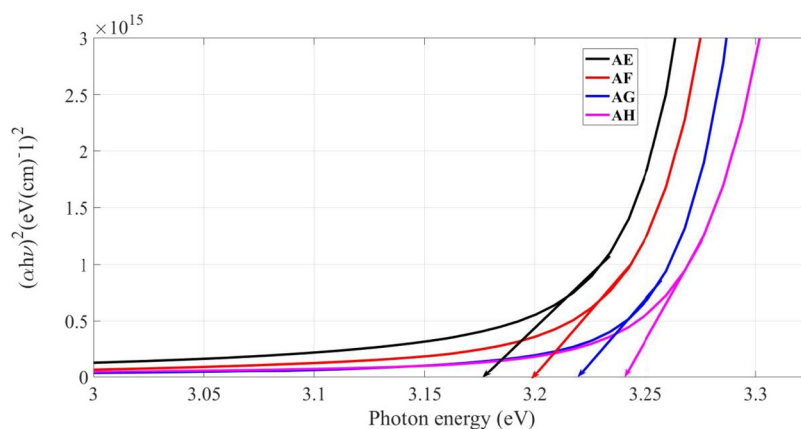


**Figure 5.** Tauc plot of pure and urea-modified ZnO thin films.

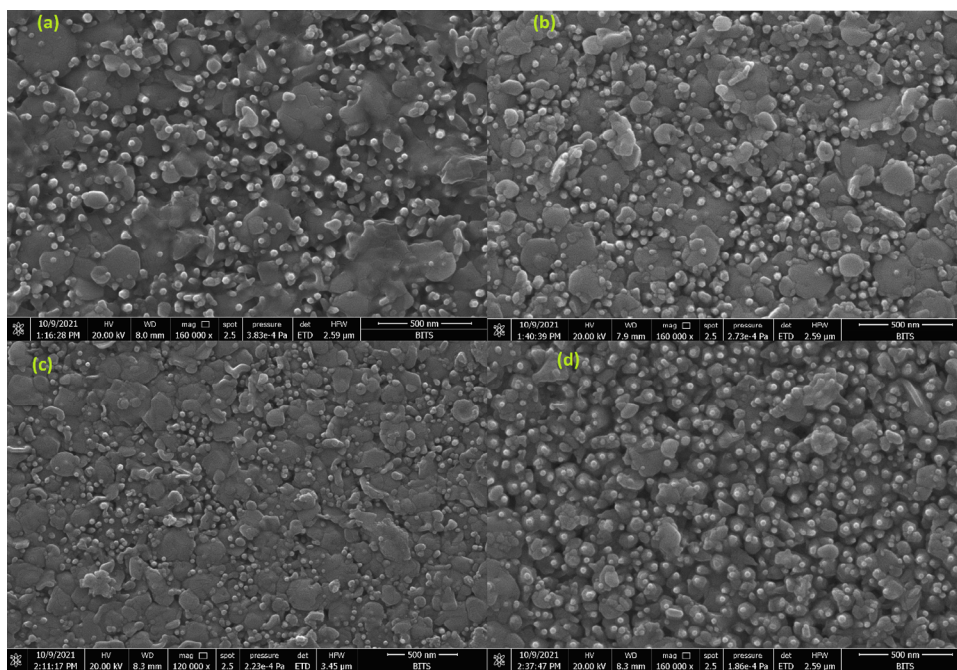


**Figure 6.** SEM images of pure and urea-modified ZnO thin films. (a) Pure ZnO, (b) 2 wt % of urea, (c) 4 wt % of urea, and (d) 6 wt % of urea.

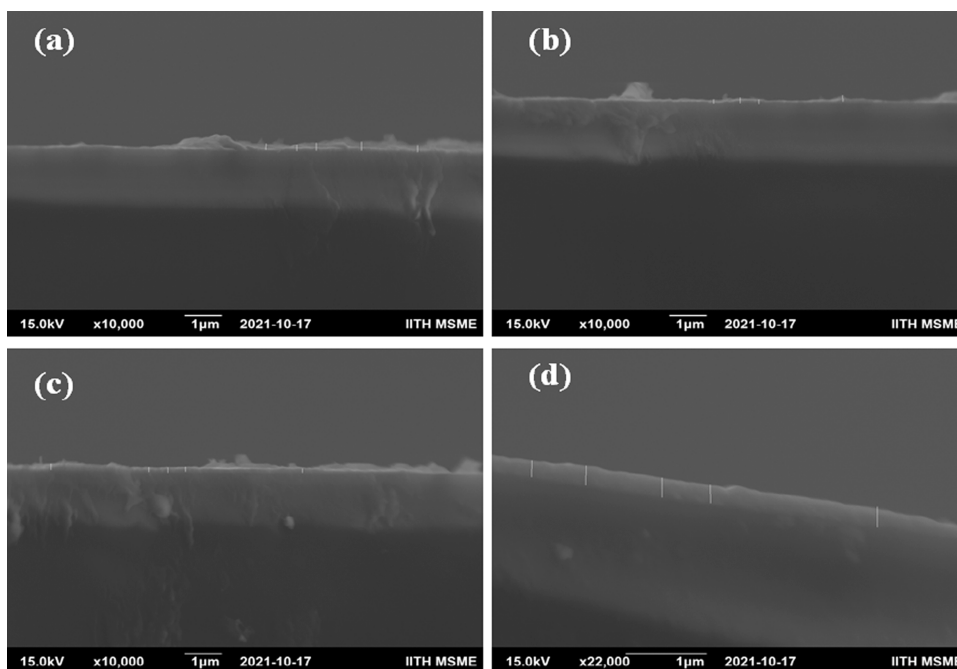


**Figure 7.** SEM cross-section view of pure and urea-modified ZnO thin films. (a) Pure ZnO, (b) 2 wt % of urea, (c) 4 wt % of urea, and (d) 6 wt % of urea.

machined surfaces. It is calculated by using the below mathematical formula.<sup>42</sup>

$$\text{Average roughness } R_a = \frac{1}{L} \int_0^L |Z(x)| dx$$

where  $Z(x)$  describes the surface profile of the sample.

The RMS roughness estimates the standard deviation of the surface height of a stipulated area, and it is used to compute the skewness of the sample.<sup>43</sup> It is described mathematically as follows.

$$\text{RMS roughness} = \sqrt{\frac{1}{L} \int_0^L |Z^2(x)| dx}$$

**Table 3** illustrates the variations of RMS roughness and average roughness for the deposited thin films. Both the RMS and average roughness increase with the precursor concentration.<sup>44</sup> The RMS roughness of pure ZnO shows the maximum value due to its large crystallite size. By increasing the urea concentration to the pure ZnO, the RMS roughness decreases in the case of 2 wt % urea-modified ZnO.

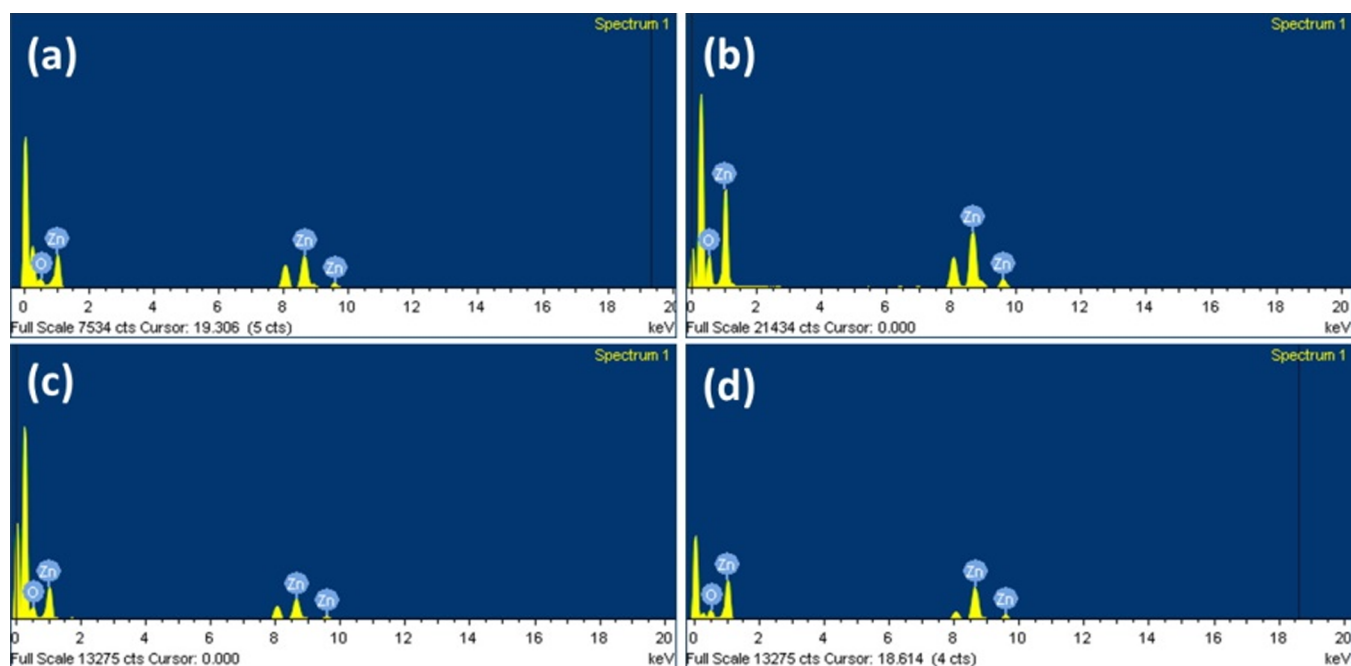


**Figure 8.** EDX results of pure and urea-modified ZnO thin films. (a) Pure ZnO, (b) 2 wt % of urea, (c) 4 wt % of urea and (d) 6 wt % of urea.

**Table 5.** EDX Analysis of Pure Zinc Oxide and Urea-Modified Zinc Oxide Thin Films

sample	zinc		oxygen	
	atomic (%)	wt (%)	atomic (%)	wt (%)
AE	77.94	93.52	22.06	6.48
AF	39.69	72.89	60.31	27.11
AG	41.01	73.96	58.99	26.04
AH	69.16	90.16	30.84	9.84

Furthermore, with increasing urea concentrations, the RMS roughness of the samples is improved. Skewness is used to demonstrate the symmetry of the variations in a particular plane/line, and this parameter is too sensitive when the plane has deep valleys and high peaks.<sup>45</sup> Negative skewness values in Table 3 indicate that valleys are preponderated on the surface and become more planer. Positive skewness represents the thin film's lopsided nature and contains more peaks than valleys.<sup>46</sup>

**3.4. Optical Studies.** A UV–vis spectrophotometer was used to study the optical characteristics of pure ZnO and urea-modified ZnO thin films at different concentrations. Figure 4 represents the room-temperature transmittance spectra of pure zinc oxide and zinc oxide thin films modified using various urea concentrations in the range of 350–750 nm. The transmittance of all samples was above 70% in the visible region, agreeing with the previously reported work.<sup>47,48</sup> It can be seen from the figure that when the wavelength ranges from 350 to 425 nm, the ZnO film modified with 2 wt % of urea shows the maximum transmittance compared with other samples. This may be due to the more voids available in the sample, which decreases the optical scattering and increases the transmittance.<sup>49</sup> When the wavelength is from 425 to 650 nm, the ZnO film modified by 2% urea does not have the maximum transmittance, but the pure ZnO film has the maximum transmittance. From 650 to 750 nm of wavelength, the 6 wt % urea-modified ZnO film has the maximum transmittance. From Beer–Lambert's law, absorbance has a logarithmic relationship with transmittance, determined by the following relation.<sup>50</sup>

$$\text{absorbance } (a) = \left(\frac{1}{d}\right) \ln\left(\frac{1}{T}\right)$$

The absorption coefficient ( $\alpha$ ) is derived with the help of absorbance values. The variation of absorption coefficient with photon energy can be explained according to the below relation.<sup>51</sup>

$$\alpha h\nu = A(h\nu - E_g)^{1/2}$$

The optical band gap is determined by plotting the  $(\alpha h\nu)^2$  versus photon energy ( $h\nu$ ), called the Tauc plot. The band gap values of the deposited samples can be estimated by using the linear part of Tauc's plot. Figure 5 represents the Tauc plot of pure and modified zinc oxide thin films with various urea concentrations. The calculated band gaps of pure ZnO thin films and urea-modified ZnO films are listed in Table 4. The optical band gap increases with increasing urea concentration due to the decrease in the thickness of the films. It might be attributed to introducing defects that create localized states in the band gap and therefore increases the band gap.<sup>52,53</sup>

**3.5. SEM.** The surface morphology of pure ZnO and urea-modified ZnO thin films was analyzed by SEM and is depicted in Figure 6. The prepared thin films' surface morphology discloses that the nanoparticles are randomly distributed by varying the grain size with different agglomeration, particle dispersion, and cluster formation. Furthermore, from Figure 6, it can be seen that the surface morphology of the sample predominantly changes with increasing concentration of urea. As a result, we conclude that urea has proven to be an effective surface modifier useful in gas sensor applications. Figure 7 depicts the cross-section view of pure and urea-modified ZnO thin films. The thickness of the samples is analyzed by Image J software, and it is obtained as 224, 208, 195, and 183 nm for AE, AF, AG, and AH samples, respectively.

The elemental analysis of the prepared pure zinc oxide and urea-modified ZnO thin films with various concentrations was done using energy-dispersive X-ray spectroscopy (EDX). This

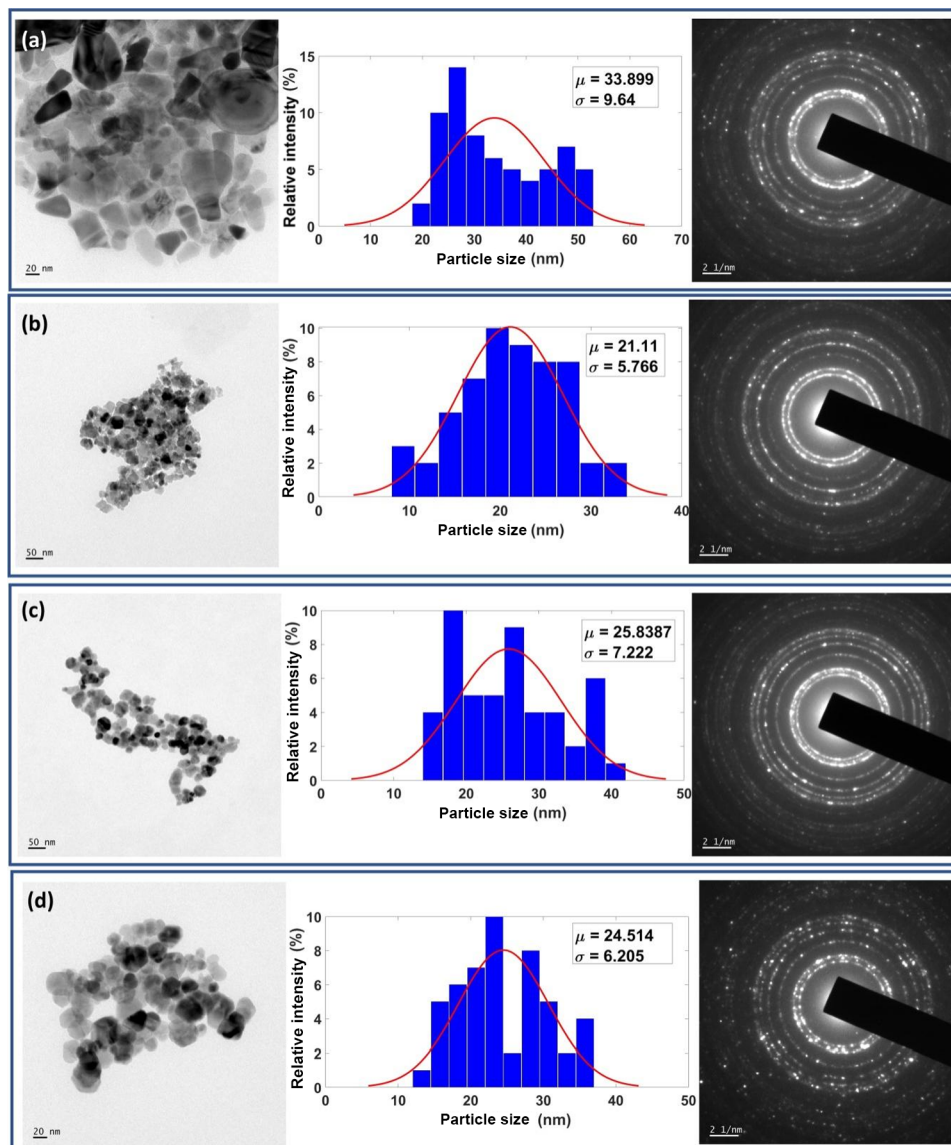


**Figure 9.** HRTEM images of zinc oxide and urea-modified zinc oxide thin films. (a) Pure ZnO, (b) 2 wt % of urea, (c) 4 wt % of urea, and (d) 6 wt % of urea.

analysis showed the presence of zinc and oxygen elements only. The EDX spectra of pristine and urea-modified ZnO thin films are depicted in Figure 8a–d. Table 5 shows that as the urea precursor concentration increases, the percentage of atomic weight of zinc increases and that of oxygen decreases. It is due to the variation in the thickness of the deposited films.<sup>54</sup>

**3.6. Transmission Electron Microscopy.** HRTEM was performed to study the size and shape of zinc oxide nanocrystallites. The conventional HRTEM and selected area electron diffraction (SAED) images of pure zinc oxide are depicted in Figure 9a and those of urea-modified ZnO nanocrystalline thin films with different concentrations are shown in Figure 9b–d. From the SAED patterns of the pure zinc oxide thin film, the bright diffraction pattern supports the hexagonal Wurtzite structure of the ZnO thin film with high crystallinity. Also, the concentric rings demonstrate the presence of an ample number of well-defined nanoparticles. The SAED pattern consists of four concentric bright diffraction rings, which are related to (101), (102), (103), and (201) reflections of the polycrystalline Wurtzite structure of zinc oxide thin films, which

is consistent with the XRD results. Figure 9b–d shows the HRTEM images of modified ZnO thin films with different concentrations of urea along with the SAED pattern. The particle size of these samples was determined using Image J and MATLAB software, and it was in the range of 33.89 nm. In contrast, the particle size was 21.11, 25.83, and 26.51 nm in the case of urea-modified ZnO thin films with different concentrations that agree with the XRD studies.

**3.7. Raman Spectroscopy.** Raman spectroscopy is a nondestructive technique to analyze the materials' bonding environment and defect-related information in nanostructured objects. Raman spectra of pure zinc oxide and urea-modified zinc oxide thin films were investigated to confirm the Wurtzite structure's existence. Figure 10 shows the Raman spectra of pure zinc oxide and urea-modified zinc oxide thin films with different urea concentrations. In all samples, common peak positions appeared at 408, 440, and 545  $\text{cm}^{-1}$  corresponding to E1(L.O.), E2(TO), and A1(A0), respectively. Among them, the E1(L.O.) mode of ZnO is associated with oxygen atoms<sup>55</sup> and E2(TO) is a

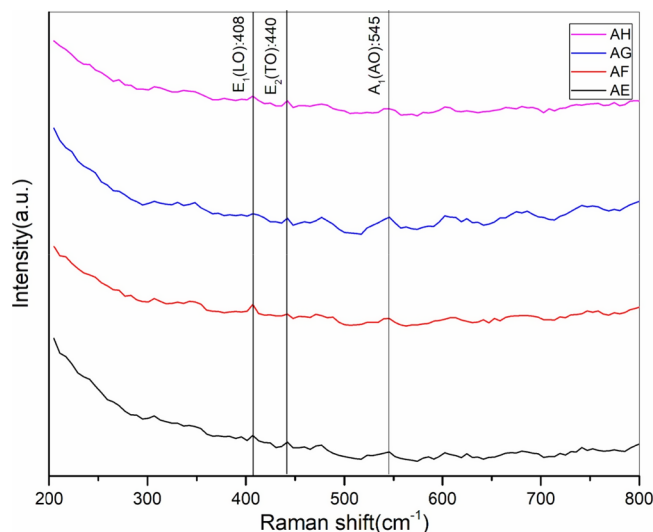


**Figure 10.** Typical Raman spectra of pure and urea-modified zinc oxide thin films.

solid narrowband which is assigned to the motion of Zn, which corresponds to the characteristic band of the Wurtzite phase.<sup>56</sup>

#### 4. GAS-SENSING CHARACTERIZATION

An indigenous gas-sensing setup and a durable electrometer (Keithley 6517 B) are used to investigate the ammonia sensing

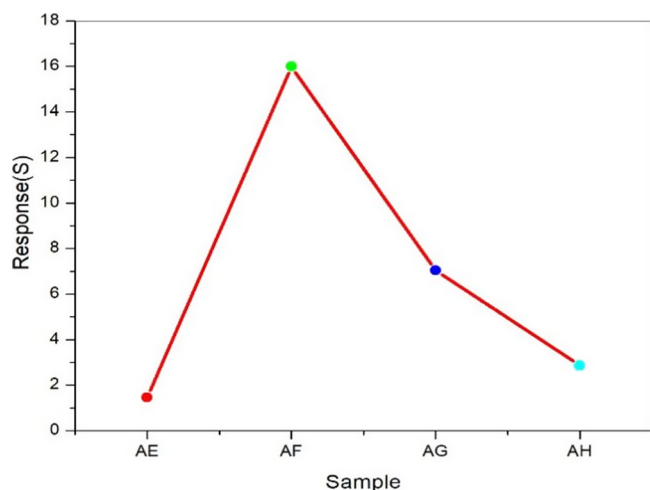


**Figure 11.** Gas response of the prepared samples.

properties of pure and urea-modified ZnO thin films at room temperature and elevated temperatures. A substrate holder is arranged to mount the thin film sensor inside the chamber (10 L stainless steel capacity). A known amount of ammonia solution is placed into a metal container inside the gas-sensing system using a microsyringe. The vapor then emits from the container and interacts with the film surface, changing the thin film's resistance. The amount of solution injected into the tube to create the required concentration of the target gas can be determined by the static liquid gas distribution technique using the following formula.<sup>57</sup>

$$C_{\text{ppm}} = \frac{22.4 \times V_1 \times \rho \times \varphi}{V_2 \times M}$$

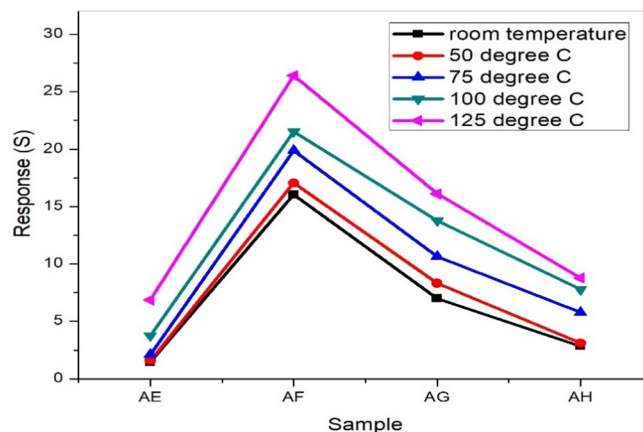


**Figure 12.** Response of pure and urea-modified ZnO thin films at different operating temperatures.

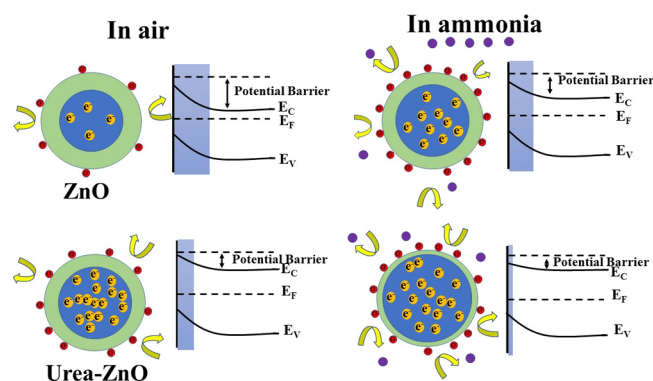


**Figure 13.** Schematic diagram of the gas-sensing mechanism.

**Table 6. Response and Recovery Times of Pure and Urea-Modified ZnO Thin Films**

s.no	sample	response time (s)	recovery time (s)
1	AE	53	85
2	AF	50	80
3	AG	65	78
4	AH	70	60

where  $C_{\text{ppm}}$  is the concentration,  $\rho$  is the density (g/mL),  $V_1$  is the volume ( $\mu\text{L}$ ),  $\varphi$  is the volume fraction,  $M$  is the molecular weight (g/mol) of the target gas, and  $V_2$  is the volume of the chamber (L).

The gas-sensing properties of metal oxide-based semiconductors depend on the reaction mechanism between the surface of the semiconductor and the test gas. ZnO is an n-type semiconductor, and its resistance may decrease in the presence of reducing gas such as ammonia. Further, the sensing area and operating temperature (room temperature) are maintained steady<sup>58</sup> for room-temperature studies. The sensitivity of the sensor element can be determined using the following equation.<sup>59</sup>

$$\text{Sensitivity} = \frac{R_{\text{air}}}{R_{\text{gas}}}$$

Figure 11 shows the sensitivity of pure zinc oxide thin films and zinc oxide thin films modified with different urea concentrations toward 25 ppm of ammonia at room temperature. The sensitivity of the sensor element is remarkably varied

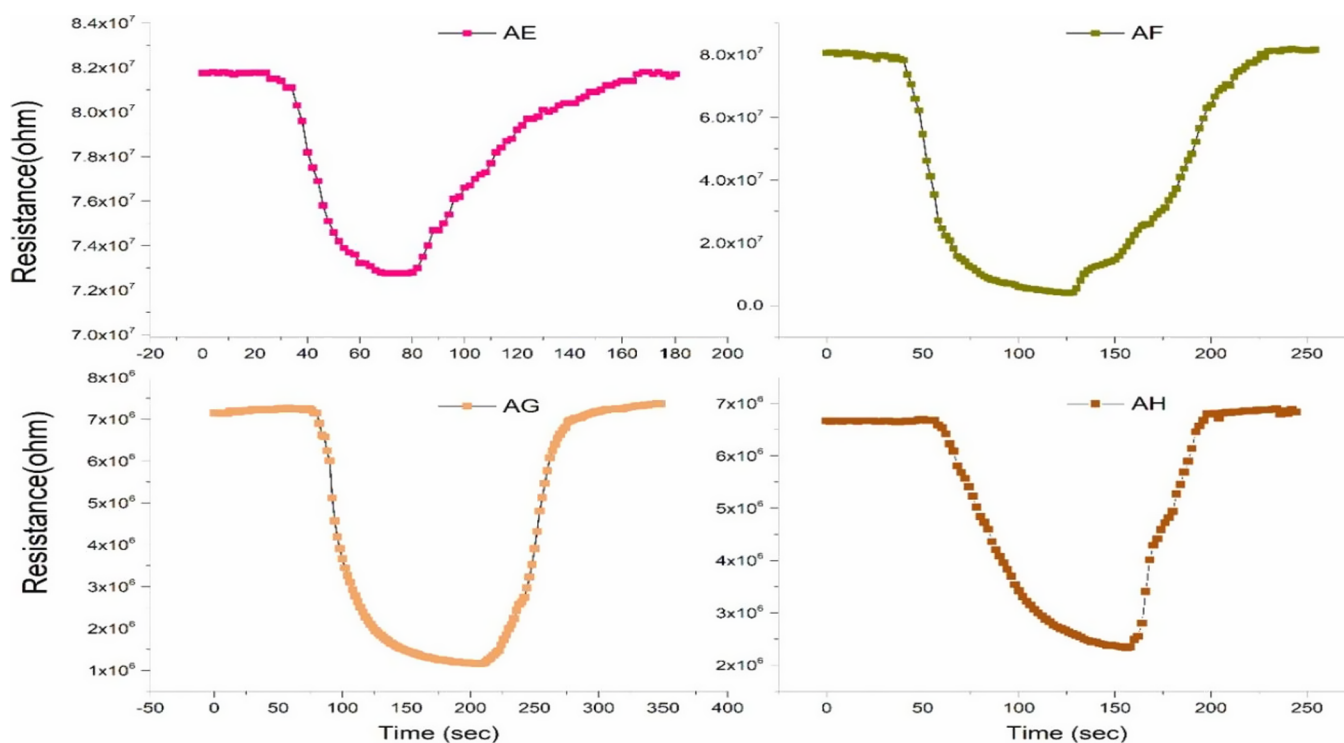
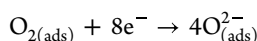
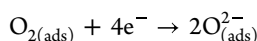
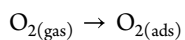


Figure 14. Transient response curves of pure and urea-modified ZnO films.

with respect to the urea concentration. The sample deposited with 2 wt % of urea has shown the maximum response toward ammonia due to the smallest crystallite size and more oxygen molecules, which will have more surface area; hence, it will provide higher active sites to enhance the gas-sensing properties. The chemisorption process, which involves both adsorption and desorption of oxygen molecules on the surface of the sensor element, is the underlying concept behind the gas detecting capabilities. Response of all sensor elements toward 25 ppm of ammonia vapors at different operating temperatures has been investigated. It is noticed that the response has been enhanced by increasing the operating temperature. The response of the sensor elements at various operating temperatures is depicted in Figure 12.

**4.1. Gas-Sensing Mechanism.** In ambient air, the oxygen molecules that exist in the air will adsorb on the surface of the sensor element and capture the free electrons from the conduction band to create  $O^-$ . When the sensor is allowed to interact with a reducing gas such as ammonia, it will react with the oxygen molecules on the surface of the ZnO sensor element, which leads to reducing the concentration of  $O^-$  ions on the surface and enhancing the concentration of electrons, thereby leading to a decrease in the resistance of the sensor element.



It is also noted that the sensor element acts as an n-type semiconductor. If the sensor element is exposed to test gas (i.e., ammonia), the chemisorbed oxygen takes out the electron from the sensor element and releases it into the conduction band. Due to this, the width of the potential barrier of the film decreases as increasing the exposure of ammonia leads to a decrease in the

sensor element's resistance.<sup>60</sup> Furthermore, when the test gas is withdrawn from the chamber, electrons are again captured by the adsorbed oxygen. This increases the resistance and returns to the original state, as shown in Figure 13.

In a step function, the sensor's reaction and recovery times are stated as the time it takes for the sensor to reach 90% of the stabilized value after acquiring or turning off the test gas. The obtained response and recovery times are tabulated in Table 6. Transient response curves of pure and urea-modified ZnO films are shown in Figure 14.

## 5. CONCLUSIONS

We have prepared pure and urea-modified zinc oxide thin films with the spray pyrolysis method using different wt % values of urea in this work. Urea plays a vital role during the solution reaction process with zinc salts, and it will provide zinc carbonate hydroxides and be converted to ZnO at elevated temperatures. The impact of urea content on the structural, morphological, optical, and gas-sensing properties has been investigated. It was found using XRD studies that the prepared samples possess polycrystalline nature with the Wurtzite structure. The crystallite size is decreased with the addition of the urea content of 2 wt %, which could inhibit ZnO's growth. SEM studies revealed a consistent surface morphology in all films, and Raman analysis confirmed the presence of Wurtzite ZnO structures. The optical band gap increases with increasing urea concentration due to the decrease in the thickness of the films. It might be attributed to introducing some defects that create localized states in the band gap and, therefore, increase it. Among all films, the ZnO thin film deposited with a urea content of 2 wt % has a small crystallite size with a high surface area, which is a promising feature in gas-sensing properties. It showed the maximum response toward 25 ppm of ammonia at room temperature with a response time of 50 s and a recovery time of 80 s.

## AUTHOR INFORMATION

### Corresponding Authors

Saidi Reddy Parne – Department of Applied Sciences, National Institute of Technology-Goa, Ponda 403401, India;

Email: [psreddy@nitgoa.ac.in](mailto:psreddy@nitgoa.ac.in)

Nagaraju Pothukanuri – Department of Physics, Sreenidhi University, Hyderabad 501301, India; [orcid.org/0000-0003-1894-6825](https://orcid.org/0000-0003-1894-6825); Email: [nagarajuphysics@gmail.com](mailto:nagarajuphysics@gmail.com)

### Authors

Venkata Satya Chidambara Swamy Vaddadi – Department of Applied Sciences, National Institute of Technology-Goa, Ponda 403401, India

Srinivasa Rao Sriram – Department of Applied Sciences, National Institute of Technology-Goa, Ponda 403401, India

Vijayakumar Yelsani – Anurag University, Hyderabad, Telangana State 500088, India

Complete contact information is available at:

<https://pubs.acs.org/10.1021/acsomega.3c00268>

### Notes

The authors declare no competing financial interest.

## ACKNOWLEDGMENTS

The authors would like to thank Dr. E.Senthamarai Kannan, Department of Physics and Kumar Kanneboyena, Central Sophisticated Instrumentation Facility, BITS-Pilani KK Birla Goa Campus, for providing SEM measurements and Raman measurements, respectively. The authors express their sincere gratitude to Mr. Talluri Manoj, research scholar, Department of Material Science and Metallurgical Engineering, IIT Hyderabad, for providing a cross-section view of SEM measurements. Dr. P.Nagaraju would like to thank the management and Prof. P.Narsimha Reddy, Pro-Chancellor, Sreenidhi University, Ghatkesar, Hyderabad, for their constant support in conducting the present research.

## REFERENCES

- (1) Nguyen, D. D.; Dang, D. V.; Nguyen, D. C. Hydrothermal synthesis and NH<sub>3</sub> gas sensing property of WO<sub>3</sub> nanorods at low temperature. *Adv. Nat. Sci. Nanosci. Nanotechnol.* **2015**, *6*, No. 035006.
- (2) Timmer, B.; Olthuis, W.; Van Den Berg, A. Ammonia sensors and their applications—a review. *Sens. Actuators B Chem.* **2005**, *10*, 666–677.
- (3) Wang, Y.; Liu, J.; Cui, X.; Gao, Y.; Ma, J.; Sun, Y.; Sun, P.; Liu, F.; Liang, X.; Zhang, T.; Lu, G. NH<sub>3</sub> gas sensing performance enhanced by Pt-loaded on mesoporous WO<sub>3</sub>. *Sens. Actuators B Chem.* **2017**, *238*, 473–481.
- (4) Christie, S.; Scorsone, E.; Persaud, K.; Kvasnik, F. Remote detection of gaseous ammonia using the near infrared transmission properties of polyaniline. *Sens. Actuators B Chem.* **2003**, *90*, 163–169.
- (5) Wang, S.; Jiang, Y.; Tai, H.; Liu, B.; Duan, Z.; Yuan, Z.; Pan, H.; Xie, G.; Xiaosong, D.; Yuanjie, S. An integrated flexible self-powered wearable respiration sensor. *Nano Energy* **2019**, *63*, No. 103829.
- (6) Shen, C. Y.; Liou, S. Y. Surface acoustic wave gas monitor for ppm ammonia detection. *Sens. Actuators B: Chem.* **2008**, *131*, 673–679.
- (7) Wang, S. Y.; Ma, J. Y.; Li, Z. J.; Su, H. Q.; Alkurd, N. R.; Zhou, W. L.; Wang, L.; Du, B.; Tang, Y. L.; Ao, D. Y.; Zhang, S. C. Surface acoustic wave ammonia sensor based on ZnO/SiO<sub>2</sub> composite film. *J. Hazard. Mater.* **2015**, *285*, 368–374.
- (8) Chen, C.; Jiang, M.; Luo, X.; Tai, H.; Jiang, Y.; Yang, M.; Xie, G.; Yuanjie, S. Ni-Co-P hollow nanobricks enabled humidity sensor for respiratory analysis and human-machine interfacing. *Sens. Actuators B Chem.* **2022**, *370*, No. 132441.
- (9) Lee, J. H. Gas sensors using hierarchical and hollow oxide nanostructures: an overview. *Sens. Actuators B Chem.* **2009**, *140*, 319–336.
- (10) Zheng, H.; Ou, J. Z.; Strano, M. S.; Kaner, R. B.; Mitchell, A.; Kalantar-Zadeh, K. Nanostructured tungsten oxide – properties, synthesis, and applications. *Adv. Funct. Mater.* **2011**, *21*, 2175–2196.
- (11) Park, J. Y.; No, Y. S.; Park, B. J.; Lee, H. W.; Choi, J. W.; Kim, J. S.; Ermakov, Y.; Yoon, S. J.; Oh, Y. J.; Choi, W. K. Low-energy ion beam treatment of  $\alpha$ -Al<sub>2</sub>O<sub>3</sub> (0001) and improvement of photo luminescence of ZnO thin films. *Met. Mater. Int.* **2004**, *10*, 351–355.
- (12) Lim, H. J.; Lee, D. Y.; Oh, Y. J. Gas sensing properties of ZnO thin films prepared by microcontact printing. *Sens. Actuators A Phys.* **2006**, *125*, 405–410.
- (13) Laurenti, M.; Garino, N.; Porro, S.; Fontana, M.; Gerbaldi, C. Zinc oxide nanostructures by chemical vapour deposition as anodes for Li-ion batteries. *J. Alloys Compd.* **2015**, *640*, 321–326.
- (14) Ismail, A. M.; Menazea, A. A.; Hoda, A. K.; El-Sherbiny, A. E.; Samy, A. The influence of calcination temperature on structural and antimicrobial characteristics of zinc oxide nanoparticles synthesized by Sole Gel method. *J. Mol. Struct.* **2019**, *1196*, 332–337.
- (15) Lupan, O.; Pauporte, T.; Chow, L.; Viana, B.; Pelle, F.; Ono, L. K.; Roldan Cuenya, B.; Heinrich, H. Effects of annealing on properties of ZnO thin films prepared by electrochemical deposition in chloride medium. *Appl. Surf. Sci.* **2010**, *256*, 1895–1907.
- (16) Prajapati, C. S.; Kushwaha, A.; Sahay, P. P. Effect of Al dopants on the structural, optical and gas sensing properties of spray-deposited ZnO thin films. *Mater. Chem. Phys.* **2013**, *142*, 276–285.
- (17) Lehrakia, N.; Aida, M. S.; Abed, S.; Attaf, N.; Attaf, A.; Poulain, M. ZnO thin films deposition by spray pyrolysis: Influence of precursor solution properties. *Curr. Appl. Phys.* **2012**, *12*, 1283–1287.
- (18) Srinivasa, R. S.; Saidi, R. P.; Nagaraju, P.; Damodar, R. E. Prospects of spray pyrolysis technique for gas sensor applications – A comprehensive review. *J. Anal. Appl. Pyrolysis* **2022**, *164*, No. 105527.
- (19) Wang, C.; Wang, E.; Shen, E.; Gao, L.; Kang, Z.; Tian, C.; Zhang, C.; Lan, Y. Growth of ZnO nanoparticles from nanowisker precursor with a simple solvothermal route. *Mater. Res. Bull.* **2006**, *41*, 2298–2302.
- (20) Hu, S. H.; Chen, Y. C.; Hwang, C. C.; Peng, C. H.; Gong, D. C. Analysis of growth parameters for hydrothermal synthesis of ZnO nanoparticles through a statistical experimental design method. *J. Mater. Sci.* **2010**, *45*, 5309–5317.
- (21) Marinho, J. Z.; Romeiro, F. C.; Lemos, S. C. S.; Motta, F. V.; Riccardi, C. S.; Li, M. S.; Longo, E.; Lima, R. C. Urea-Based Synthesis of Zinc Oxide Nanostructures at Low Temperature. *J. Nanomater.* **2012**, *2012*, 1–7.
- (22) Li, Y.; Jian-er, Z.; Larbot, A.; Persin, M. Preparation and characterization of nano-zinc oxide. *J. Mater. Process.* **2007**, *189*, 379–383.
- (23) Nagaraju, P.; Vijayakumar, Y.; Reddy, G. L. N.; Ramana Reddy, M. V. ZnO wrinkled nanostructures: enhanced BTX sensing. *J. Mater. Sci.: Mater. Electron.* **2018**, *29*, 11457–11465.
- (24) Hong, Y.; Ryu, H.; Lee, W.-J. Effects of Urea as an Additive in Fe<sub>2</sub>O<sub>3</sub> Thin-Film Photoelectrodes. *Electron. Mater. Lett.* **2019**, *15*, 733–742.
- (25) Patil, V. L.; Kumbhar, S. S.; Vanalakar, S. A.; Tarwal, N. L.; Mali, S. S.; Kim, J. H.; Patil, P. S. Gas sensing properties of 3D mesoporous nanostructured ZnO thin films. *New J. Chem.* **2018**, *42*, 13573–13580.
- (26) Uysal, B.; Sen, S.; Top, A. Photocatalytic and optical properties of zinc oxide structures prepared at different urea concentrations. *Rev. Romana Mater.* **2020**, *50*, 463–470.
- (27) Lu, J.; Zhang, Q.; Wang, J.; Saito, F.; Uchida, M. Synthesis of N-Doped ZnO by grinding and subsequent heating ZnO urea mixture. *Powder Technol.* **2006**, *162*, 33–37.
- (28) Varudkar, H. A.; Umadevi, G.; Nagaraju, P.; Dargad, J. S.; Mote, V. D. Fabrication of Al-doped ZnO nanoparticles and their application as a semiconductor-based gas sensor for the detection of ammonia. *J. Mater. Sci.: Mater. Electron.* **2020**, *31*, 12579–12585.

- (29) Bhat, P.; Nagaraju, P. Synthesis and characterization of ZnO-MWCNT nanocomposites for 1-butanol sensing application at room temperature. *Phys. B* **2019**, *570*, 139–147.
- (30) Bindu, P.; Thomas, S. Estimation of lattice strain in ZnO nanoparticles: X-ray peak profile analysis. *J. Theor. Appl. Phys.* **2014**, *8*, 123–134.
- (31) Manjunath, G.; Nagaraju, P.; Saumen, M. Ultra-sensitive clogging free combustible molecular precursor-based screen-printed ZnO sensors: a detection of ammonia and formaldehyde breath markers. *J. Mater. Sci.: Mater. Electron.* **2021**, *32*, 5713–5728.
- (32) Sharma, N.; Kumar, S.; Kumar, J. Synthesis and structural properties of ZnO doped nanoparticles prepared by hydrothermal method. *Integr. Ferroelectr.* **2018**, *186*, 115–119.
- (33) Nagaraju, P.; Vijayakumar, Y.; Choudhary, R. J.; Ramana Reddy, M. V. Preparation and characterization of nanostructured Gd doped cerium oxide thin films by pulsed laser deposition for acetone sensor application. *Mater. Sci. Eng., B* **2017**, *226*, 99–106.
- (34) Ayeb, K.; Moussa, N.; Nsib, M. F. ZnO modified by urea–hydrogen peroxide adduct as photocatalyst for 2-propanol photo-oxidation in the gas phase under different irradiations. *Reac. Kinet. Mech. Catal.* **2020**, *129*, 1103–1113.
- (35) Khoshhesab, Z. M.; Sarfaraz, M.; Houshyar, Z. Influences of Urea on Preparation of Zinc Oxide Nanostructures Through Chemical Precipitation in Ammonium Hydrogencarbonate Solution. *Synth. React. Inorg., Met.-Org., Nano-Met. Chem.* **2012**, *42*, 1363–1368.
- (36) Sharma, A.; Rai, V. N.; Mani, S.; Chawade, S. A study of structural parameters and photoluminescence of Tb doped ZnO nanoparticles. *Mater. Today Proc.* **2020**, *26*, 58–63.
- (37) Bhat, P.; Naveen Kumar, S. K.; Nagaraju, P. Fabrication of ultrasensitive hexagonal disc structured ZnO thin film sensor to trace nitric oxide. *J. Asian Ceram. Soc.* **2021**, *9*, 96–105.
- (38) Sunil Gavaskar, D.; Nagaraju, P.; Vijayakumar, Y.; Reddy, P. S.; Ramana Reddy, M. V. Low-cost ultra-sensitive SnO<sub>2</sub>-based ammonia sensor synthesized by hydrothermal method. *J. Asian Ceram. Soc.* **2020**, *8*, 605–614.
- (39) Raoufi, D.; Kiasatpour, A.; Fallah, H. R.; Rozatian, A. S. H. Surface characterization and microstructure of ITO thin films at different annealing temperatures. *Appl. Surf. Sci.* **2007**, *253*, 9085–9090.
- (40) Kumar, B. R.; Rao, T. S. AFM studies on surface morphology, topography and texture of nanostructured zinc aluminium oxide thin films. *Dig. J. Nanomater. Biostruct.* **2012**, *7*, 1881–1889.
- (41) De Oliveira, R.R.L.; Albuquerque, D.A.C.; Cruz, T.G.S.; Yamaji, F.M.; Leite, F.L.; Measurement of the nanoscale roughness by atomic force microscopy: basic principles and applications. In *Atomic Force Microscopy Imaging, Measuring and Manipulating Surfaces at the Atomic Scale*, 5th ed.; Victor, B., Ed.; InTech: Europe, 2012, *3*, 147–174.
- (42) Bajpai, A. K.; Bhatt, R.; Katare, R. Atomic force microscopy enabled roughness analysis of nanostructured poly (diamino naphthalene) doped poly (vinyl alcohol) conducting polymer thin films. *Micron* **2016**, *90*, 12–17.
- (43) Vijayakumar, Y.; Nagaraju, P.; Veeraswamy, Y.; Reddy, P. S.; Nasser, S. A.; Ramana Reddy, M. V. Nanostructured Al and Fe co-doped ZnO thin films for enhanced ammonia detection. *Phys. B* **2020**, *581*, No. 411976.
- (44) Xu, L.; Li, Z.; Cai, Q.; Wang, H.; Gao, H.; Lv, W.; Liu, J. Precursor template synthesis of three-dimensional mesoporous ZnO hierarchical structures and their photocatalytic properties. *CrystEngComm* **2010**, *12*, 2166–2172.
- (45) Leach, R. K. Traceable measurement of surface texture at the National Physical Laboratory using NanoSurf IV. *Meas. Sci. Technol.* **2000**, *11*, 1162–1172.
- (46) Tudose, I. V.; Horvath, P.; Suche, M.; Christoulakis, S.; Kitsopoulos, T.; Kiriakidis, G. Correlation of ZnO thin film surface properties with conductivity. *J. Appl. Phys.* **2007**, *89*, 57–61.
- (47) Jabeen, M.; Ishaq, M.; Song, W.; Xu, L.; Maqsood, I.; Deng, Q. UV-assisted photocatalytic synthesis of ZnO-reduced graphene oxide nanocomposites with enhanced photocatalytic performance in degradation of methylene blue. *ECS J. Solid State Sci. Technol.* **2017**, *6*, 36–43.
- (48) Longo, A.; Verucchi, R.; Aversa, L.; Tatti, R.; Ambrosio, A.; Orabona, E.; Coscia, U.; Carotenuto, G.; Maddalena, P. Graphene oxide prepared by graphene nanoplatelets and reduced by laser treatment. *Nanotechnology* **2017**, *28*, No. 224002.
- (49) Babu, B. J.; Maldonado, A.; Velumani, S.; Asomoza, R. Electrical and optical properties of ultrasonically sprayed Al-doped zinc oxide thin films. *Mater. Sci. Eng., B* **2010**, *174*, 31–37.
- (50) Nagaraju, P.; Vijayakumar, Y.; Phase, D. M.; Choudary, R. J.; Ramana Reddy, M. V. Microstructural, optical and gas sensing characterization of laser ablated nanostructured ceria thin films. *J. Mater. Sci.: Mater. Electron.* **2016**, *27*, 651–658.
- (51) Nagaraju, P.; Vijayakumar, Y.; Radhika, P.; Choudary, R. J.; Ramana Reddy, M. V. Structural, morphological, optical and gas sensing properties of nanocrystalline ceria thin films. *Mater. Today* **2016**, *3*, 4009–4018.
- (52) Varnamkhandi, M. G.; Fallah, H. R.; Mostajabodavati, M.; Hassanzadeh, A. Influence of Ag thickness on electrical, optical and structural properties of nanocrystalline MoO<sub>3</sub>/Ag/ITO multilayer for optoelectronic applications. *Vacuum* **2012**, *86*, 1318–1322.
- (53) Ben Rabeh, M.; Khedmi, N.; Fodha, M. A.; Kanzari, M. The Effect of Thickness on Optical Band Gap and N-type Conductivity of CuInS<sub>2</sub> Thin Films Annealed in Air Atmosphere. *Energy Procedia* **2014**, *44*, 52–60.
- (54) Roguai, S.; Djelloul, A. A structural and optical properties of Cu-doped ZnO films prepared by spray pyrolysis. *Appl. Phys. A: Mater. Sci. Process.* **2020**, *126*, 122.
- (55) Kaviyarasu, K.; Maria Magdalane, C.; Kanimozhi, K.; Kennedy, J.; Siddhardha, B.; Subba Reddy, E.; Naresh, K. R.; Chandra, S. S.; Thema, F. T.; Douglas, L.; Genene, T. M.; Maaza, M. Elucidation of Photocatalysis, Photoluminescence and Antibacterial studies of ZnO thin films by spin coating method. *J. Photochem. Photobiol. B Biol.* **2017**, *173*, 466–475.
- (56) Li, C.; Lv, Y.; Guo, L.; Xu, H.; Ai, X.; Zhang, J. Raman and excitonic photoluminescence characterizations of ZnO star shaped nanocrystals. *J. Lumin.* **2007**, *122*, 415–417.
- (57) Feng, C. H.; Kou, X. Y.; Chen, B.; Qian, G. B.; Sun, Y. F.; Lu, G. Y. One-pot synthesis of In doped NiO nanofibers and their gas sensing properties. *Sens. Actuators, B: Chem.* **2017**, *253*, 584–591.
- (58) Radhi Devi, K.; Selvan, G.; Karunakaran, M.; Loyola Poul Raj, I.; Ganesh, V.; AlFaify, S. Enhanced room temperature ammonia gas sensing properties of strontium doped ZnO thin films by cost-effective SILAR method. *Mater. Sci. Semicond. Process.* **2020**, *119*, No. 105117.
- (59) Nagaraju, P.; Vijayakumar, Y.; Ramana Reddy, M. V. Room-temperature BTEX sensing characterization of nanostructured ZnO thin films. *J. Asian Ceram. Soc.* **2019**, *7*, 141–146.
- (60) Vijayakumar, Y.; Nagaraju, P.; Sreekanth, T.; Rushidhar, U.; Reddy, P. S. Effect of precursor volume on chemically sprayed V<sub>2</sub>O<sub>5</sub> thin films for acetaldehyde detection. *Superlattices Microstruct.* **2021**, *153*, No. 106870.